Supporting Information

Significantly enhanced NIR emission of solid-state clusters based on Cu_4Pt_2 triggered with volatile organic compounds

Xue-Ning Hu,[a†] Xu-Hang Zhong,[a†] Rui-Ru Zhong,[a] Lin-Mei Zhang,[a] De-Bo Hao,[a] Qian Xu,[a] Hui-Zhi Wei,[a] Rui Zhou,[a,b] Jianyu Wei,[c] Kuan-Guan Liu,[c] Shang-Fu Yuan,*[a] Dong-Sheng Li,[d] and Tao Wu*[a]

[a]College of Chemistry and Materials Science, and Guangdong Provincial Key Laboratory of Functional Supramolecular Coordination Materials and Applications, Jinan University, Guangzhou 510632, P. R. China.

[b]Department of Developmental and Regenerative Biology, Jinan University, Guangzhou, 510632, P. R. China.

[c]Ningxia Key Laboratory for Photovoltaic Materials, School of Materials and New Energy, Ningxia University, Yinchuan, Ningxia 750021, China.

[d]College of Materials and Chemical Engineering, Hubei Provincial Collaborative Innovation Center for New Energy Microgrid, Key Laboratory of Inorganic Nonmetallic Crystalline and Energy Conversion Materials, China Three Gorges University, Yichang, 443002, P. R. China.

E-mail: sfyuan@jnu.edu.cn; wutao@jnu.edu.cn.

†These authors contributed equally to this work.

I. Supporting figures

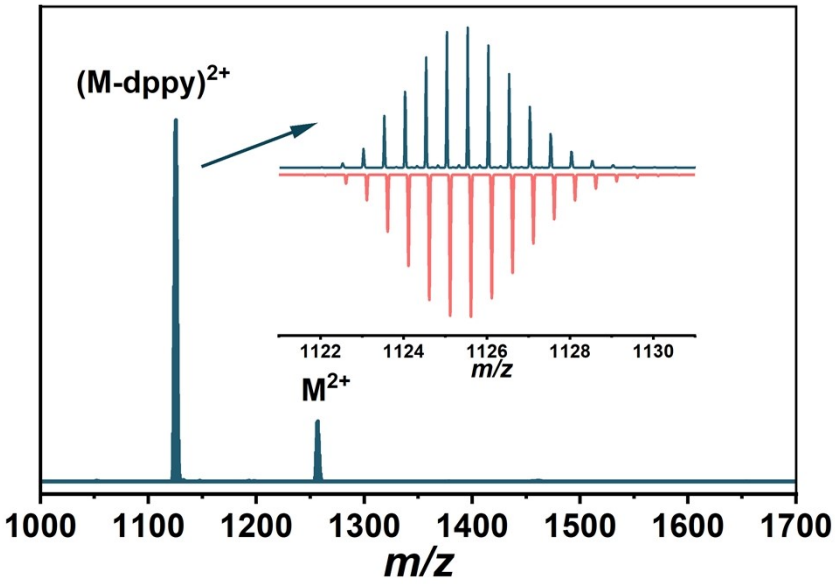

Figure S1. ESI-MS spectra of **CZ-Cu_4Pt_2**. M = $[Cu_4Pt_2(CZ\text{-}PrA)_4(dppy)_3]$. Inset: the measured (blue trace) and simulated (red trace) isotopic distribution patterns of fragment ion peak $(M\text{-}dppy)^{2+}$.

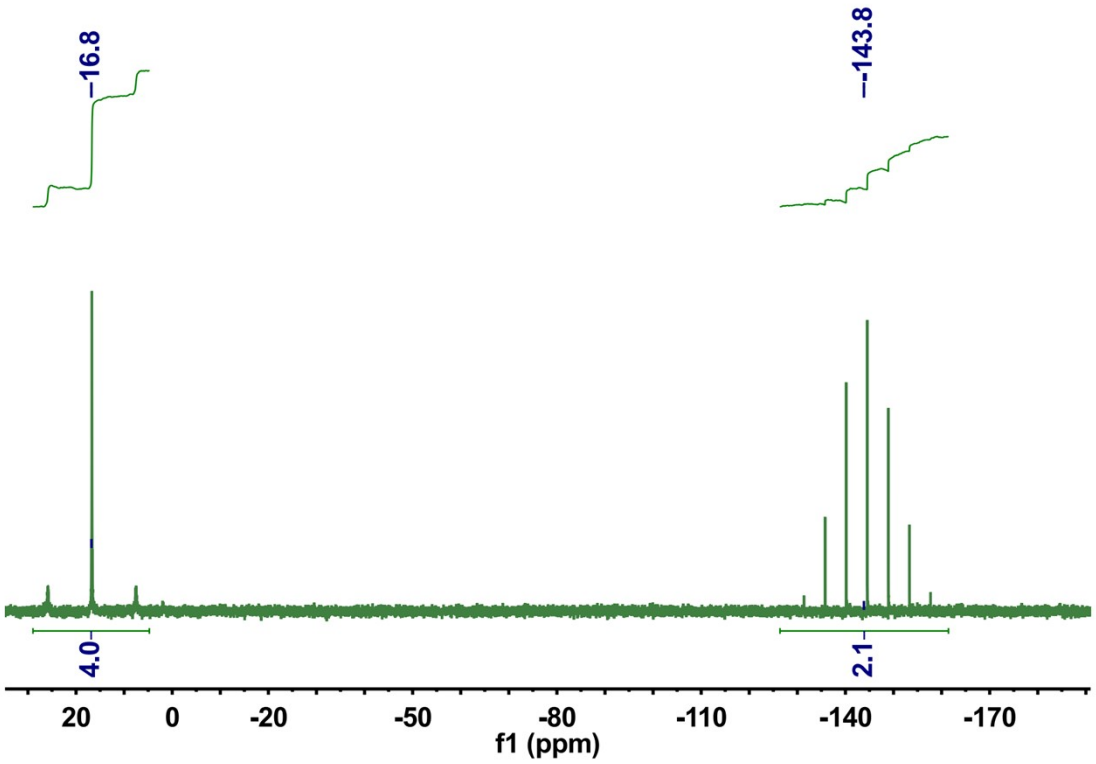

Figure S2. ^{31}P NMR spectra of **CZ-Cu$_4$Pt$_2$**.

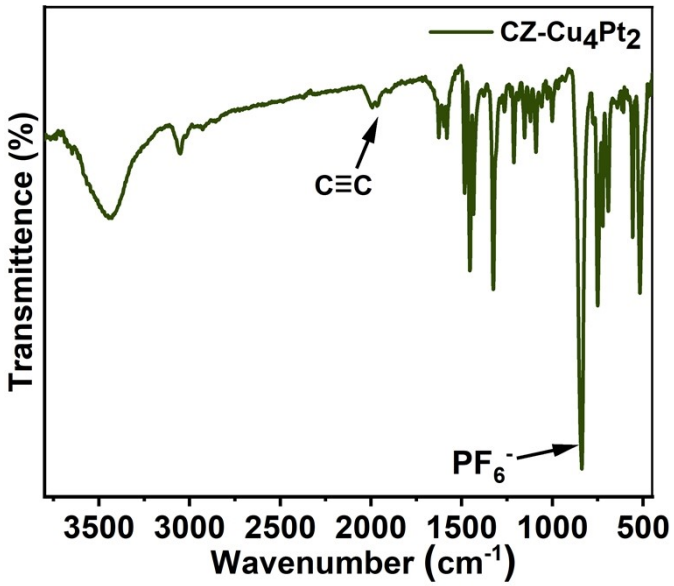

Figure S3. FT-IR spectra of **CZ-Cu$_4$Pt$_2$**.

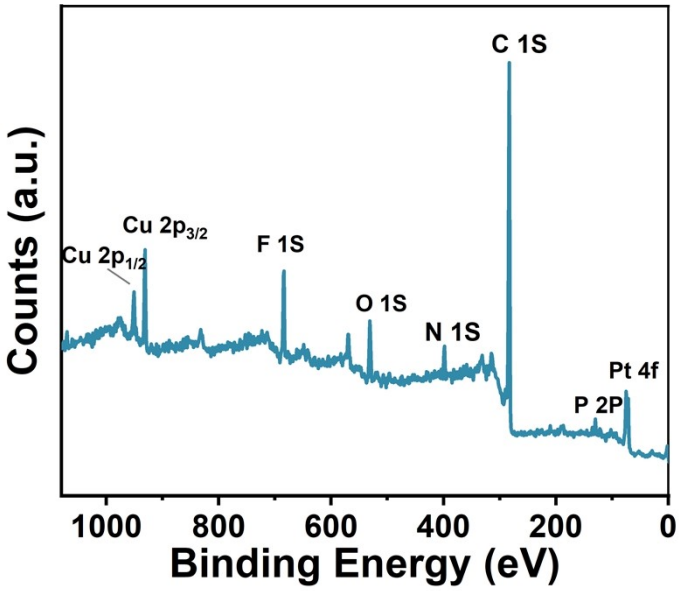

Figure S4. XPS full spectrum of **CZ-Cu_4Pt_2**.

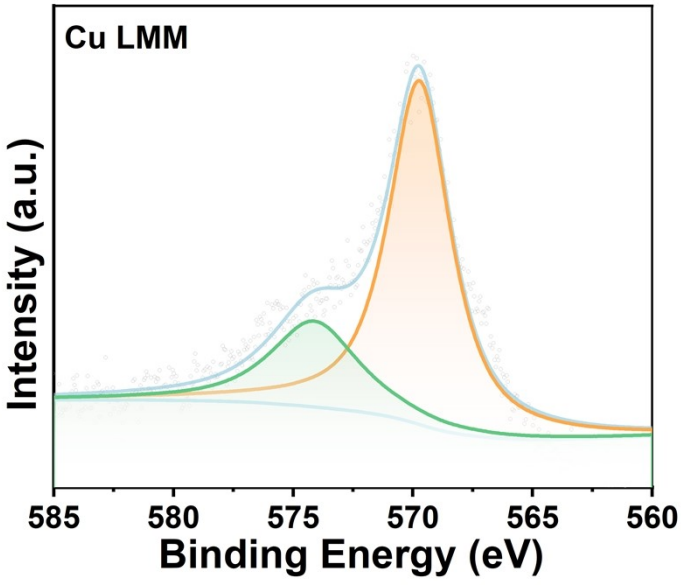

Figure S5. Cu LMM spectrum of **CZ-Cu_4Pt_2**.

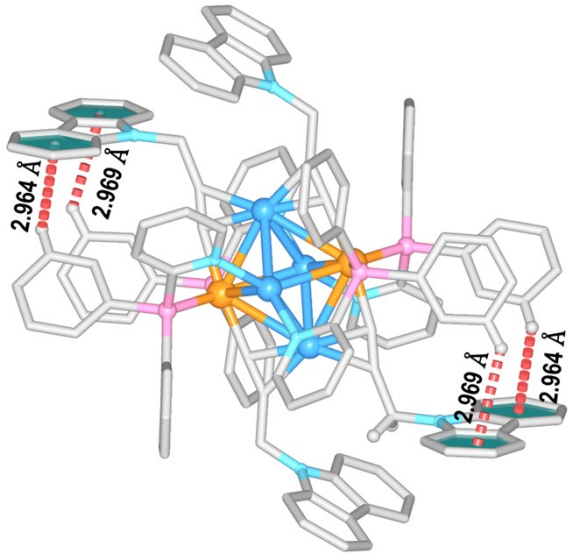

Figure S6. The intramolecular interactions (C-H···π) in **MeO-Cu$_4$Pt$_2$**.

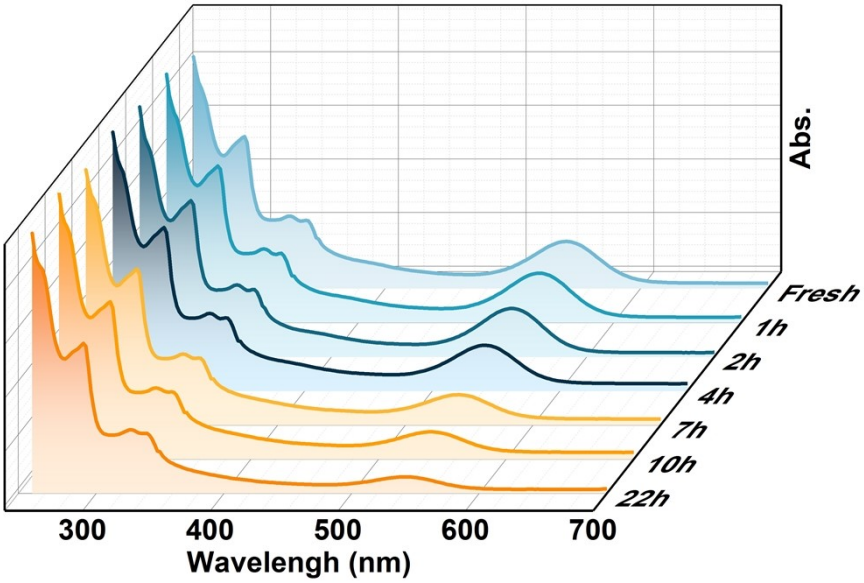

Figure S7. Monitoring solution-state stability of **CZ-Cu$_4$Pt$_2$** in CH_2Cl_2 under ambient conditions (25℃ in air).

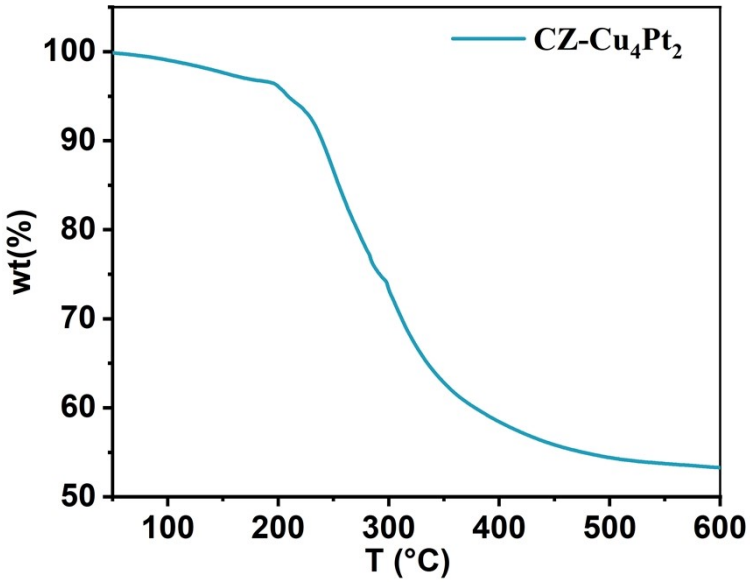

Figure S8. Thermogravimetric analysis (TGA) of **CZ-Cu$_4$Pt$_2$**.

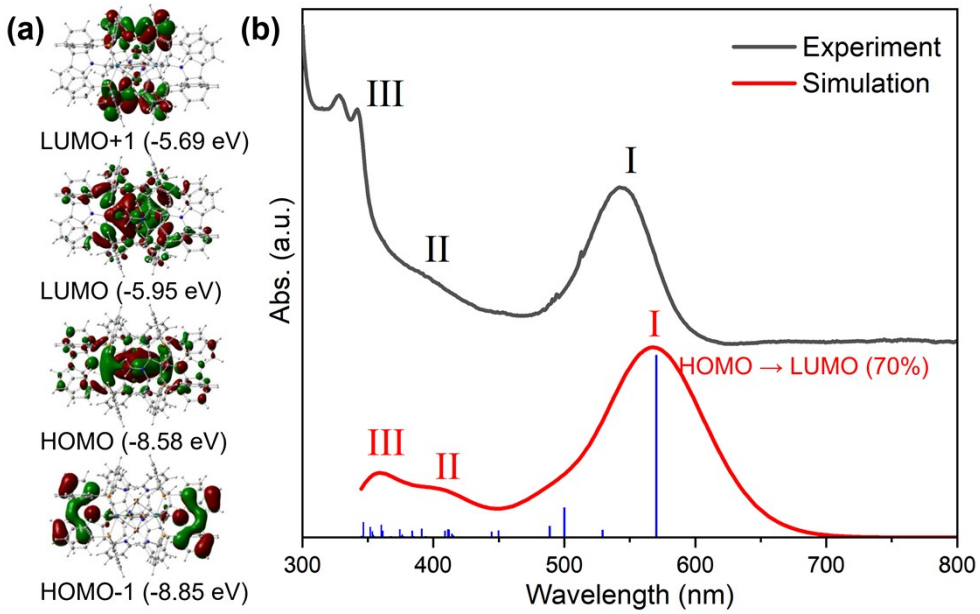

Figure S9. The plots of the frontier MOs of **CZ-Cu$_4$Pt$_2$** (a). Experimental and simulated UV-vis spectra of **CZ-Cu$_4$Pt$_2$**. The blue sticks represented the computed oscillator strengths (b).

Density functional theory (DFT) calculations were performed by using Gaussian 16 package.[1] The generalized gradient approximation (GGA) Becke-Perdew (BP86) exchange-correlation functional,[2,3] together with an all-electron Def2-SVP[4] basis set were used for the geometry optimization. Dispersion forces were considered via the empirical pairwise corrections of Grimme (DFT-D3).[5] The optimized structures were

confirmed as true minima on their potential energy surface by analytical vibrational frequency calculations. The orbital energies were re-calculated by taking BP86/Def2-SVP optimized geometry as single point at B3LYP[6] level. Excitation energies of the first 100 excited states was calculated by using TD-DFT[7] approach under B3LYP/Def2-SVP level of theory. The UV−vis spectrum was simulated from the computed transition energies and their oscillator strength where each transition being associated with a Gaussian function of half-height width equal to 1300 cm^{-1}, a value that best reproduces the experimental spectrum.

The optimized geometry was found to be of C_i symmetry, with a reasonably large HOMO-LUMO gap of 2.63 eV calculated under B3LYP/Def2-SVP level of theory. The DFT optimized metal-metal distances are comparable to those measured from the X-ray structure. The HOMO-1 belongs to the alkynyl ligands and shown a π(carbazolyl) nature (Figure S9a). The HOMO and LUMO levels are mainly distributed in the octahedral Cu_4Pt_2 metallic core, exhibiting Cu(3d)/Pt(5d) and Cu(4s+4p)/Pt(6s+6p) characters, respectively. The LUMO+1 is made of the phosphine orbitals displaying π*(phenyl) nature. The absorption spectrum of **CZ-Cu_4Pt_2** was simulated by TD-DFT calculation, in which the excitation energies and oscillator strengths of the first 100 excited states were computed. The simulated UV−vis spectrum is in a good agreement with the experimental one (Figure S9b). The first absorption band (I at 565 nm) is mainly corresponded to the HOMO → LUMO transition which show a MMCT nature. The two higher energy bands (II at 410 nm; III at 355 nm) are associated with several LMCT and LLCT involved the π(carbazolyl)-, Cu(4s+4p)/Pt(6s+6p)- and π*(phenyl)-type MOs.

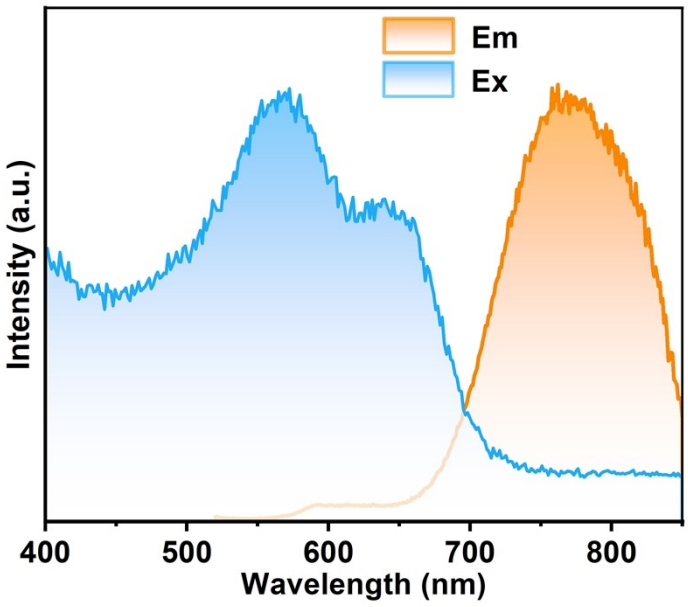

Figure S10. The PL excitation and emission spectra of **CZ-Cu_4Pt_2** in the DCM.

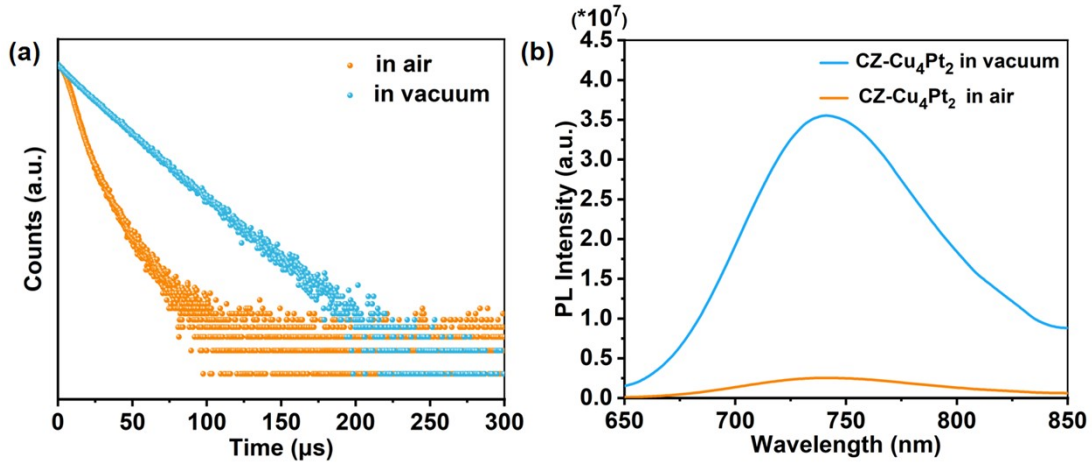

Figure S11. (a) PL decay profile and (b) NIR emission spectra of **CZ-Cu_4Pt_2** under vacuum and ambient conditions.

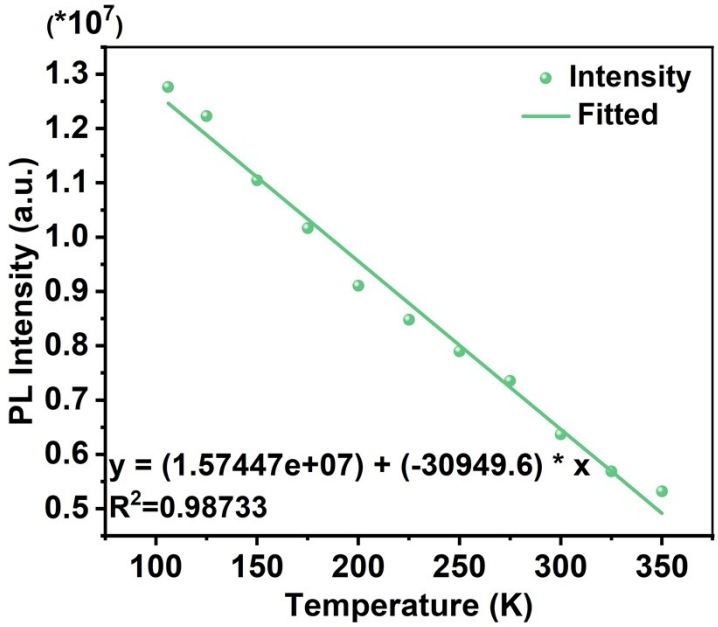

Figure S12. Emission intensity data fitting with Temperature for **CZ-Cu_4Pt_2**.

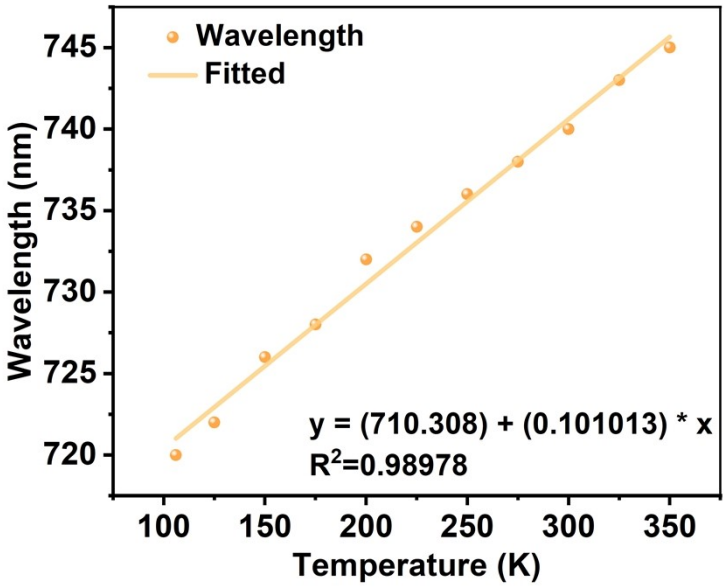

Figure S13. Emission peak wavelength data fitting with Temperature for **CZ-Cu_4Pt_2**.

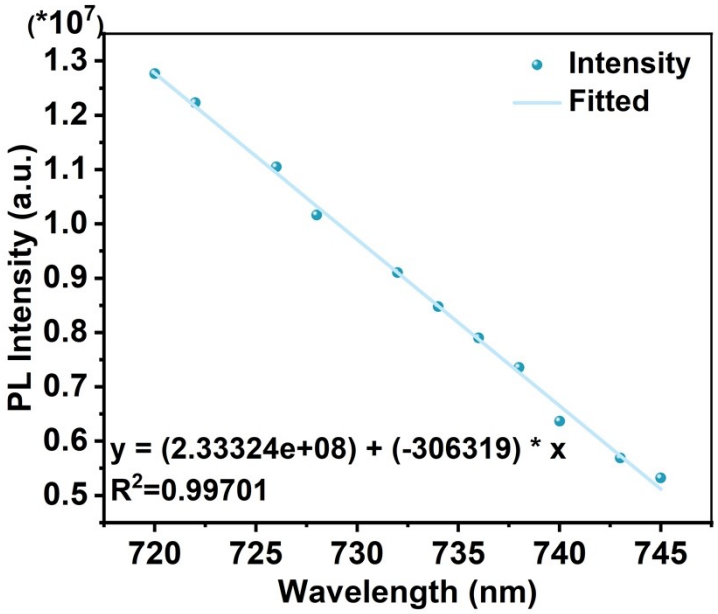

Figure S14. Emission intensity data fitting with peak wavelength for **CZ-Cu_4Pt_2**.

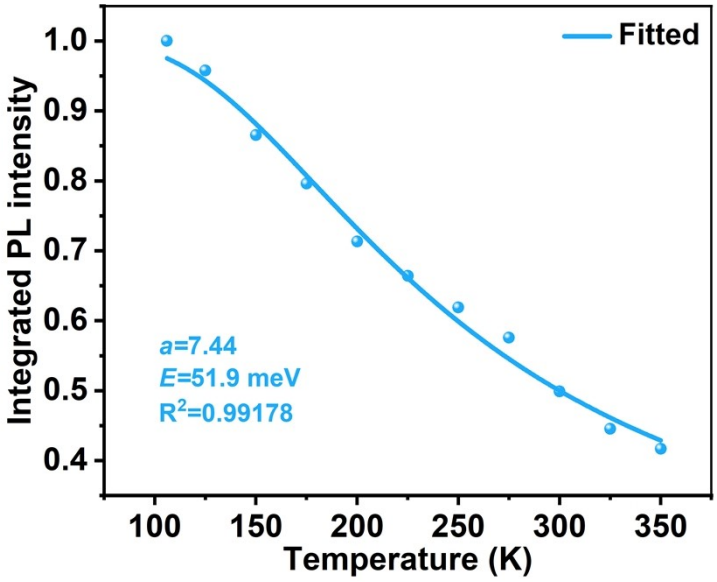

Figure S15. Normalized integrated PL intensities and fitting using Eq. 3 (data from variable-temperature PL spectra of **CZ-Cu_4Pt_2**).

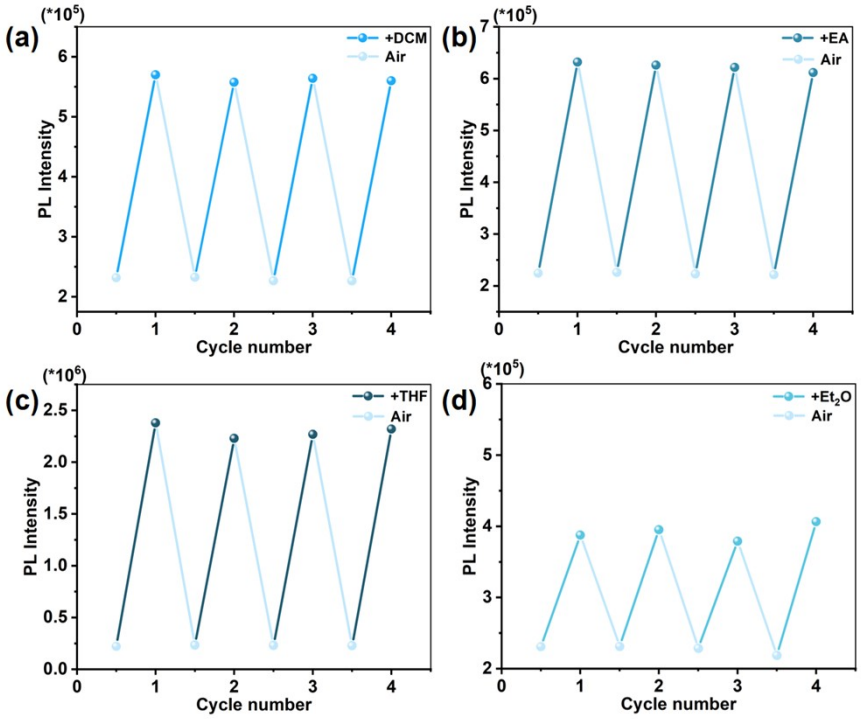

Figure S16. PL emission response cycle of **CZ-Cu_4Pt_2** under solvent vapor stimulus. The dark lines indicate the solvent interaction process, while the light lines represent the drying process.

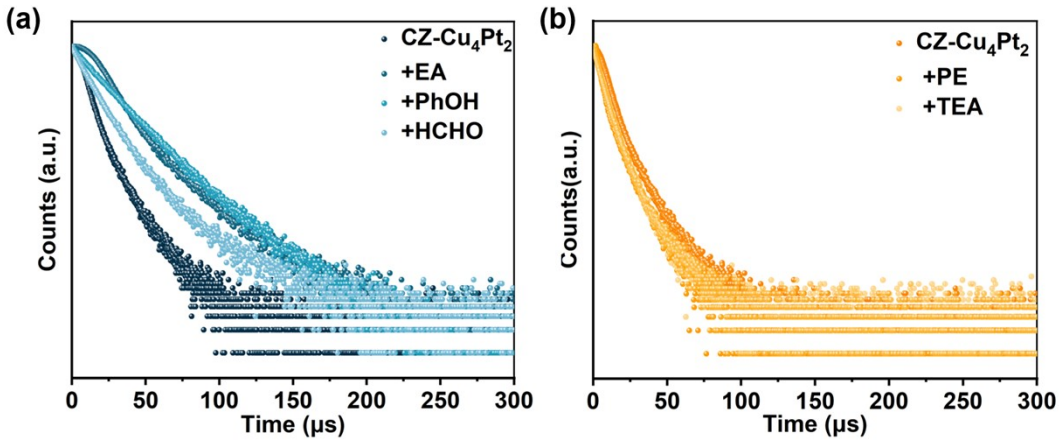

Figure S17. PL decay profile of **CZ-Cu$_4$Pt$_2$** before and after immersed in various solvents (λ_{ex} = 500 nm).

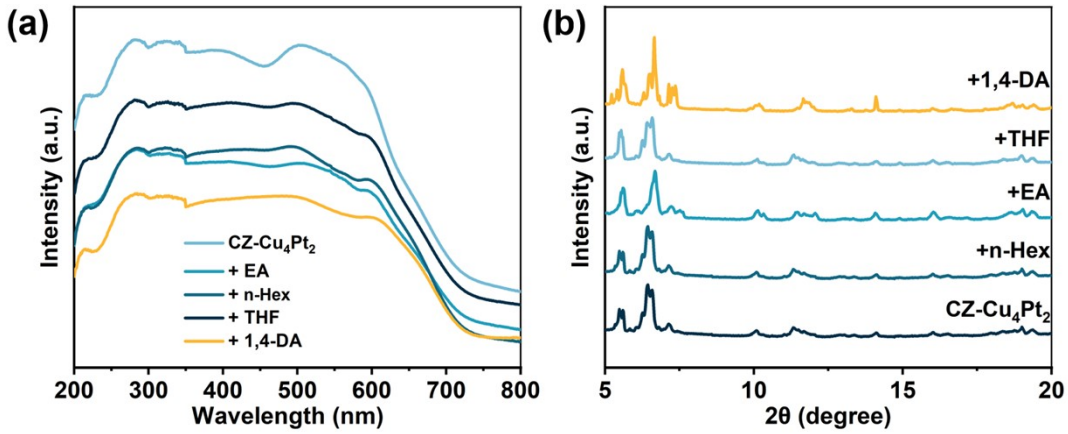

Figure S18. (A) UV–vis DRS and (B) PXRD of **CZ-Cu$_4$Pt$_2$** before and after immersed in various solvents.

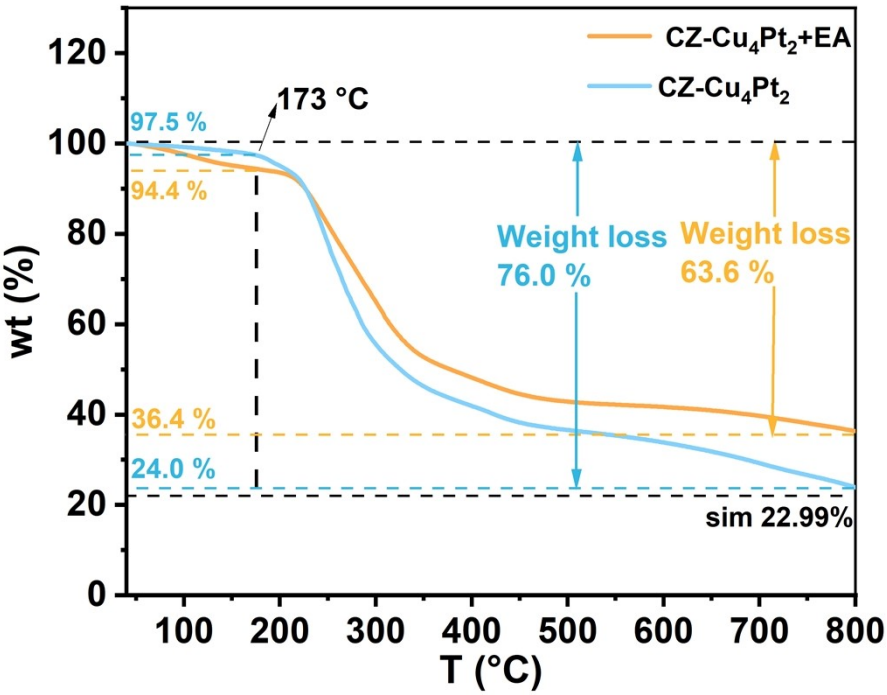

Figure S19. Comparison of TGA for **CZ-Cu$_4$Pt$_2$** and **CZ-Cu$_4$Pt$_2$**⊃EA.

The blue line in Fig. S19 represents the weight loss process of **CZ-Cu$_4$Pt$_2$**, showing a 2.5% weight loss between 40–173°C, which can be attributed to the presence of dichloromethane and moisture. The orange line represents the weight loss of **CZ-Cu$_4$Pt$_2$**⊃EA, showing a greater weight loss between 40–173°C, followed by a clear plateau at 173°C, indicating that the EA molecules were completely lost at this temperature. Despite the boiling point of EA being 77°C, its complete loss at 173°C suggested strong intermolecular interactions between EA and the cluster molecules. The total weight loss at 173°C is 5.6%, which includes EA, dichloromethane, and moisture. The difference in weight loss between the two samples indicated that the EA molecules account for 3.4% of the total weight of **CZ-Cu$_4$Pt$_2$**. This suggested that each **CZ-Cu$_4$Pt$_2$** molecule contains approximately 1.08 EA molecules. At 800°C, the remaining weight of **CZ-Cu$_4$Pt$_2$** is 24.0%, which is close to the simulated value of 22.9%. However, the presence of EA may cause the **CZ-Cu$_4$Pt$_2$**⊃EA to generate metal oxides during heating, resulting in a higher residual weight compared to **CZ-Cu$_4$Pt$_2$**.

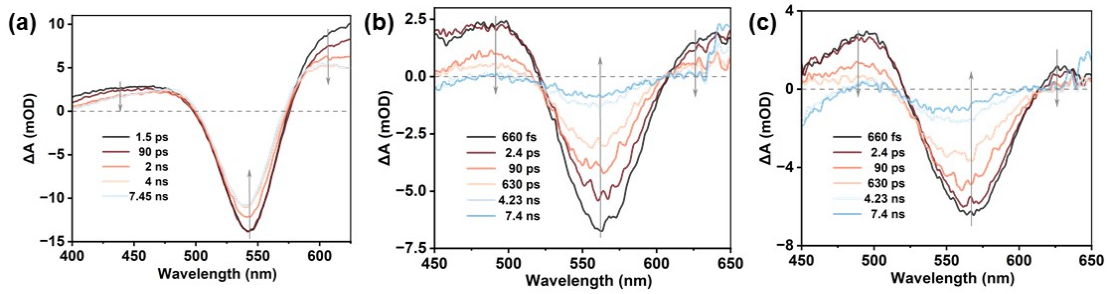

Figure S20. fs-TA spectra at selected time delays for (a) **CZ-Cu$_4$Pt$_2$** in DCM solution, (b) **CZ-Cu$_4$Pt$_2$**, and (c) **CZ-Cu$_4$Pt$_2$**⊃PhCl.

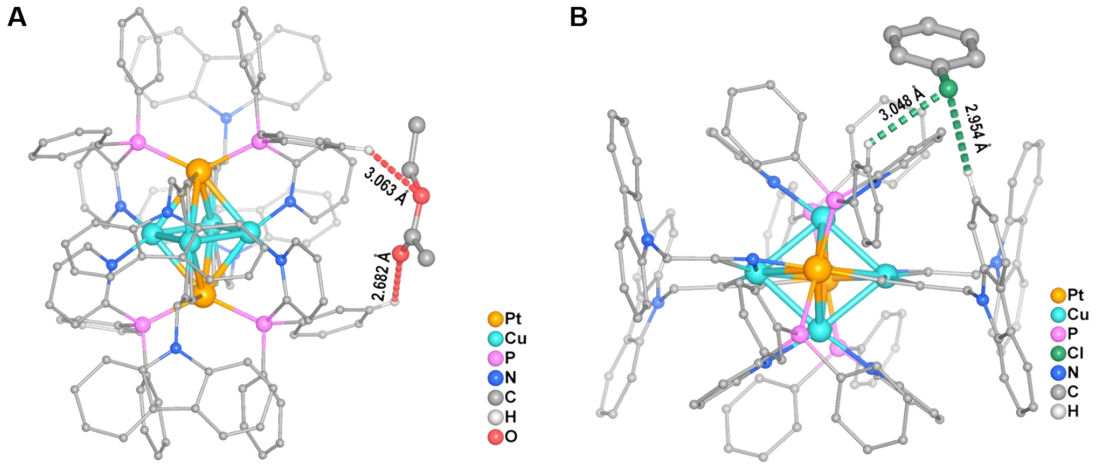

Figure S21. (A) X-ray diffraction single crystal pattern of **CZ-Cu$_4$Pt$_2$** after exposure to ethyl acetate. (B) X-ray diffraction single crystal pattern of **CZ-Cu$_4$Pt$_2$** after exposure to chlorobenzene.

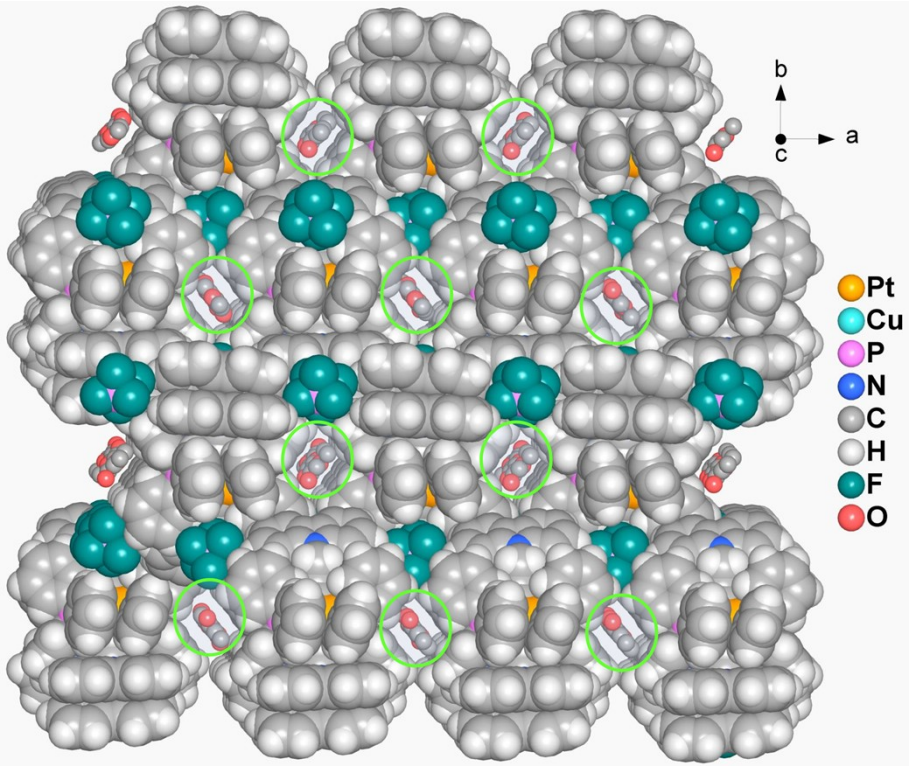

Figure S22. Molecular packing of **CZ-Cu_4Pt_2**⊃EA, highlighting the one-dimensional channel of EA molecules (green circles).

Table S1. Crystal data and structure refinement for **CZ-Cu_4Pt_2**.

Identification code	CZ-Cu_4Pt_2
Empirical formula	$C_{130}H_{100}N_8F_{12}P_6Cl_4Cu_4Pt_2$
Formula weight	2974.13
Temperature/K	99.96(18)
Crystal system	monoclinic
Space group	$P2_1/n$
a/Å	14.4294(3)
b/Å	24.0473(4)
c/Å	18.0186(4)
α/°	90
β/°	92.752(2)
γ/°	90
Volume/Å^3	6245.0(2)
Z	2
ρ_{calc} g/cm^3	1.582
μ/mm^{-1}	6.919
F(000)	2948.0
Crystal size/mm^3	0.2 × 0.16 × 0.14
Radiation	Cu Kα (λ = 1.54184)
2Θ range for data collection/°	7.15 to 124.996
Index ranges	$-16 \le h \le 16$, $-27 \le k \le 27$, $-17 \le l \le 20$
Reflections collected	21366
Independent reflections	9663 [R_{int} = 0.0482, R_{sigma} = 0.0611]
Data/restraints/parameters	9663/258/775
Goodness-of-fit on F^2	1.191
Final R indexes [I>=2σ (I)]	R_1 = 0.1151, wR_2 = 0.2978
Final R indexes [all data]	R_1 = 0.1220, wR_2 = 0.3013
Largest diff. peak/hole / e Å^{-3}	5.30/-1.77

Table S2. Crystal data and structure refinement for **CZ-Cu_4Pt_2⊃**EA.

Identification code	CZ-Cu_4Pt_2⊃EA
Empirical formula	$C_{134}H_{108}N_8O_2F_{12}P_6Cl_4Cu_4Pt_2$
Formula weight	3062.21
Temperature/K	100.0(2)
Crystal system	monoclinic
Space group	$P2_1/n$
a/Å	14.7492(7)
b/Å	23.9210(6)
c/Å	17.9965(5)
α/°	90
β/°	90.991(3)
γ/°	90
Volume/Å^3	6348.5(4)
Z	2
ρ_{calc} g/cm^3	1.506
μ/mm^{-1}	6.043
F(000)	2854.0
Crystal size/mm^3	0.2 × 0.15 × 0.10
Radiation	Cu Kα (λ = 1.54184)
2Θ range for data collection/°	7.686 to 129.988
Index ranges	$-17 \le h \le 17$, $-25 \le k \le 28$, $-17 \le l \le 21$
Reflections collected	40382
Independent reflections	10733 [R_{int} = 0.0612, R_{sigma} = 0.0486]
Data/restraints/parameters	10733/286/758
Goodness-of-fit on F^2	1.464
Final R indexes [I>=2σ (I)]	R_1 = 0.1124, wR_2 = 0.3268
Final R indexes [all data]	R_1 = 0.1233, wR_2 = 0.3355
Largest diff. peak/hole / e Å^{-3}	5.80/-2.08

Table S3 Lifetime of **CZ-Cu_4Pt_2** under different temperature.

Temperature (K)	100	125	150	175	200	225
Lifetime (μs)	12.17	12.18	12.53	12.42	12.46	12.58
Temperature (K)	250	275	300	325	350	
Lifetime (μs)	12.43	12.55	12.20	12.11	12.29	

Table S4 Photophysical parameters of **CZ-Cu_4Pt_2** in the original state and after the addition of various solvents.

Cluster	QY /%	Lifetime /μs	k_r /s^{-1}	k_{nr} /s^{-1}
CZ-Cu_4Pt_2	16.1	5.39	$2.98*10^4$	$1.56*10^5$
CZ-Cu_4Pt_2⊃n-Hex	22.4	7.58	$2.95*10^4$	$1.02*10^5$
CZ-Cu_4Pt_2⊃EA	46.7	12.75	$3.66*10^4$	$4.18*10^4$
CZ-Cu_4Pt_2⊃THF	62.7	10.00	$6.27*10^4$	$3.73*10^4$
CZ-Cu_4Pt_2⊃PhCl	65.3	9.90	$6.60*10^4$	$3.41*10^4$
CZ-Cu_4Pt_2⊃HCHO	70.3	10.46	$6.72*10^4$	$2.84*10^4$

Table S5 Lifetime (τ_i) and amplitudes (A_i) of the transient absorption decays at 625 nm for **CZ-Cu_4Pt_2** and **CZ-Cu_4Pt_2**⊃PhCl (pump = 330 nm).

λ = 625 nm	τ_1 (ps)	A_1 (%)	τ_2 (ps)	A_2 (%)	τ_3 (ps)	A_3 (%)
CZ-Cu_4Pt_2	0.27±0.04	1.76	42.59±4.79	4.67	2006.3±210.7	93.57
CZ-Cu_4Pt_2⊃PhCl	0.43±0.09	3.53	20.68±8.31	7.70	153.08±57.76	88.77

References:

1. Frisch, M. J.; Trucks, G. W.; Schlegel, H. B.; Scuseria, G. E.; Robb, M. A.; Cheeseman, J. R.; Scalmani, G.; Barone, V.; Petersson, G. A.; Nakatsuji, H.; Li, X.; Caricato, M.; Marenich, A. V.; Bloino, J.; Janesko, B. G.; Gomperts, R.; Mennucci, B.; Hratchian, H. P.; Ortiz, J. V.; Izmaylov, A. F.; Sonnenberg, J. L.; Williams-Young, D.; Ding, F.; Lipparini, F.; Egidi, F.; Goings, J.; Peng, B.; Petrone, A.; Henderson, T.; Ranasinghe, D.; Zakrzewski, V. G.; Gao, J.; Rega, N.; Zheng, G.; Liang, W.; Hada, M.; Ehara, M.; Toyota, K.; Fukuda, R.; Hasegawa, J.; Ishida, M.; Nakajima, T.; Honda, Y.; Kitao, O.; Nakai, H.; Vreven, T.; Throssell, K.; Montgomery, J. A., Jr.; Peralta, J. E.; Ogliaro, F.; Bearpark, M. J.; Heyd, J. J.; Brothers, E. N.; Kudin, K. N.; Staroverov, V. N.; Keith, T. A.; Kobayashi, R.; Normand, J.; Raghavachari, K.; Rendell, A. P.; Burant, J. C.; Iyengar, S. S.; Tomasi, J.; Cossi, M.; Millam, J. M.; Klene, M.; Adamo, C.; Cammi, R.; Ochterski, J. W.; Martin, R. L.; Morokuma, K.; Farkas, O.; Foresman, J. B.; Fox, D. J. *Gaussian16*, Gaussian, Inc.: Wallingford, CT, **2016**.

2. Becke, A. D. Density-Functional Exchange-Energy Approximation with Correct Asymptotic Behavior. *Phys. Rev. A* **1988**, *38*, 3098− 3100

3. Perdew, J. P. Density-Functional Approximation for the Correlation Energy of the Inhomogeneous Electron Gas. *Phys. Rev. B* **1986**, *33*, 8822−8824.

4. Weigend, F.; Ahlrichs, R. Balanced Basis Sets of Split Valence, Triple Zeta Valence and Quadruple Zeta Valence Quality for H to Rn: Design and Assessment of Accuracy. *Phys. Chem. Chem. Phys.* **2005**, *7*, 3297−3305.

5. Grimme, S. Semiempirical GGA-type density functional constructed with a long-range dispersion correction. *J. Comput. Chem*. **2006**, *27*, 1787–1799.

6. A. D. Becke, “Density-functional thermochemistry. III. The role of exact exchange,” *J. Chem. Phys.* **1993**, *98*, 5648-5652.

7. Runge, E.; Gross, E. K. U. Density-functional theory for timedependent systems. *Phys. Rev. Lett.* **1984**, *52*, 997−1000.